Plasma Science and Technology

PAPER

Theoretical simulation study of laser-induced plasma bombardment on bacteria

To cite this article: Junxiao WANG *et al* 2024 *Plasma Sci. Technol.* **26** 105503

Plasma Sci. Technol. **26** (2024) 105503 (7pp) https://doi.org/10.1088/2058-6272/ad5adb

Theoretical simulation study of laser-induced plasma bombardment on bacteria

Junxiao WANG (王俊霄)[1,2], **Yan ZHANG** (张岩)[3], **Wanfei ZHANG** (张婉飞)[4], **Yong GUO** (郭勇)[4], **Lei ZHANG** (张雷)[1,2,*], **Zefu YE** (叶泽甫)[5], **Zhujun ZHU** (朱竹军)[5], **Wangbao YIN** (尹王保)[1,2,*] **and Suotang JIA** (贾锁堂)[1,2]

[1] State Key Laboratory of Quantum Optics and Quantum Optics Devices, Institute of Laser Spectroscopy, Shanxi University, Taiyuan 030006, People's Republic of China
[2] Collaborative Innovation Center of Extreme Optics, Shanxi University, Taiyuan 030006, People's Republic of China
[3] School of Optoelectronic Engineering, Xi'an Technological University, Xian 710021, People's Republic of China
[4] Shanxi Xinhua Chemical Defense Equipment Research Institute Co. Ltd., Taiyuan 030008, People's Republic of China
[5] Shanxi Gemeng US-China Clean Energy R & D Center Co. Ltd., Taiyuan 030032, People's Republic of China

[*]E-mail of corresponding authors: k1226@sxu.edu.cn and ywb65@sxu.edu.cn

Received 1 March 2024, revised 20 June 2024
Accepted for publication 21 June 2024
Published 30 August 2024

Abstract

With the rapid advancement of laser decontamination technology and growing awareness of microbial hazards, it becomes crucial to employ theoretical model to simulate and evaluate decontamination processes by laser-induced plasma. This study employs a two-dimensional axisymmetric fluid dynamics model to simulate the power density of plasma bombardment on bacteria and access its decontamination effects. The model considers the transport processes of vapor plasma and background gas molecules. Based on the destructive impact of high-speed moving particles in the plasma on bacteria, we investigate the bombardment power density under various conditions, including different laser spot sizes, wavelengths, plate's tilt angles, and plate-target spacing. The results reveal that the bombardment power density increases with a decrease in laser spot size and wavelength. For instance, when the plate is parallel to the target surface with a 1 mm spacing, the bombardment power density triples as the laser spot size decreases from 0.8 mm to 0.5 mm and quadruples as the wavelength decreases from 1064 nm to 266 nm. Notably, when the plate is parallel to the target with a relatively close spacing of 0.5 mm, the bombardment power density at 0° inclination increases sevenfold compared to 45°. This simulation study is essential for optimizing optical parameters and designing component layouts in decontamination devices using laser-induced plasma. The reduction of laser spot size, wavelength, plate-target spacing and aligning the plate parallel to the target, collectively contribute to achieving precise and effective decontamination.

Keywords: laser-induced breakdown spectroscopy, fluid dynamics model, bacterial decontamination

(Some figures may appear in colour only in the online journal)

1. Introduction

Harmful bacteria, recognized as potential biochemical

[*] Authors to whom any correspondence should be addressed.

weapons, pose a significant threat to national public security and defense equipment. The development of rapid, efficient, and environmentally friendly decontamination technology is imperative for the advancement of emerging national equipment. Traditional chemical decontamination methods primarily rely on wet decontamination [1, 2], but they present challenges such as secondary pollution, making them unsuitable for surfaces of electronic equipment, precision instruments, sensitive materials, etc. Physical decontamination methods, including ultraviolet, gamma ray, X-ray, microwave, and ultrasonic [3–7], suffer from drawbacks such as prolonged processes, radiation hazards, or unsatisfactory decontamination effects. Laser-induced plasma decontamination is grounded in laser-induced breakdown spectroscopy (LIBS) technology [8, 9]. When the energy density of the laser pulse surpasses the breakdown threshold of the target, the affected area on the target surface instantly evaporates, forming plasma through the ionization of the vapor. The resulting plasma contains energetic electrons, ions, molecules, free radicals, and other active particles capable of disrupting the cell structure and DNA/RNA of bacteria, leading to bacterial death. Compared to traditional methods, laser-induced plasma decontamination offers advantages such as high efficiency, strong penetration, safety, and pollution-free characteristics. It emerges as a standout solution among existing microbial decontamination methods.

In recent decades, extensive research has been conducted globally on the direct bacterial decontamination using lasers. For example, Shukla *et al* utilized a nanosecond infrared carbon dioxide laser to remove skin cells and bacteria beneath a micrometer-thick liquid layer, and found that laser fluence exceeding the boiling threshold of the liquid resulted in the removal of the liquid layer [10]. Grishkanich *et al* used ultraviolet laser radiation to inactivate pathogenic viruses in water, demonstrating its effectiveness against coliforms and enteric viruses [11]. Terlep *et al* proposed an Er:YAG photoacoustic irrigation technology based on super short pulses, achieving the removal of 92% of Enterococcus faecalis biofilms on a titanium surface within 10 s. This method significantly reduced the number of viable bacteria remaining on the surface [12]. Jang *et al* utilized a 266-nm UV laser to eliminate Bacillus atrophaeus spores on ceramic tiles and assessed the sterilization efficiency in relation to water absorption, tile color, and surface brightness. Results showed that matte, white, and vitrified tiles exhibited the highest sterilization efficiency, which positively correlated with the number of UV laser exposures and laser intensity [13]. However, there are limited reports on utilizing laser-induced plasma for bacterial removal. Kawasaki *et al* studied the sterilization effect of pulsed laser ablation plasma using a thin film deposition system. They used a pulsed laser with an energy density of 9.3 J/cm^2 to ablate a silver target, and one minute of plasma irradiation effectively inactivated yeast fungus and spore-forming bacteria. Sterilization efficacy depended on laser fluence and irradiation time, with high-energy silver atoms and ions considered as the main sterilization factors [14]. They also confirmed that plasmas generated by pulsed laser ablation of Ti and TiO_2 targets effectively killed yeast fungus and spore-forming bacteria, with the former showing superior efficacy [15]. Recently, we have also conducted research on bacterial recognition and decontamination based on LIBS. The average identification rate for seven bacteria reached 98.9%, with inactivation rates exceeding 98% for Escherichia coli and Bacillus subtilis [16, 17].

Given that improper handling of bacterial samples in sterilization experiments may lead to infection or disease among researchers, theoretical simulation of the bacterial decontamination process by laser-induced plasma is of significant importance for guiding experimental research and optimizing parameters. In this study, we simulate the sterilization process of laser-induced plasma using two-dimensional axisymmetric fluid dynamics equations, and focus on exploring the effects of laser spot size, wavelength, plate's tilt angle, and plate-target spacing on the bombardment power density of plasma acting on bacteria.

2. Theoretical model

In this study, the total energy of the laser is 100 mJ, and the background gas is argon at one atmospheric pressure. We theoretically simulate the bombardment power density of the plasma generated by laser ablation of the alloy target on bacteria. During the modeling process, our primary focus is on the inactivation mechanism of high-energy particles in the plasma on bacteria, which includes the effects of moving particles and thermal effects. However, we have neglected the oxidation reactions involving reactive oxygen ions and free radicals in the plasma with proteins and nucleic acids in bacteria, as well as the ultraviolet radiation mechanism of the plasma.

2.1. Heating of the target

When a high-energy pulse laser irradiates the target material, the temperature of the target material begins to increase, leading to melting as it absorbs laser energy. The heating process of the target material can be described using the following heat conduction equation [18, 19]:

$$c_{\mathrm{p}}\rho_{\mathrm{s}}\left(\frac{\partial T_{\mathrm{s}}}{\partial t}-v\frac{\partial T_{\mathrm{s}}}{\partial z}\right)=\lambda_{\mathrm{s}}\frac{\partial^2 T_{\mathrm{s}}}{\partial z^2}+(1-R)\alpha I\exp(-\alpha z), \qquad (1)$$

where c_{p}, ρ_{s}, λ_{s}, R and α are the specific heat, mass density, thermal conductivity, reflectivity, and absorption coefficient of the sample, respectively, T_{s} is the temperature of the sample, v is the evaporation rate, I is the laser power density reaching the sample surface after considering the shielding effect, and z is the coordinate along the inward normal to the sample. We assume that the specific heat is constant, which overestimates the energy of the plasma and introduces a 3% uncertainty that can be disregarded.

2.2. Generation and expansion of plasma

When the temperature of the target material reaches its boiling point, it will evaporate to form vapor. The particles in the vapor will continue to absorb laser energy and become ionized, forming a plasma. The process of plasma expanding outward can be described by fluid dynamics equations. Considering the interaction between vapor plasma and background gas, mass diffusion, viscosity, and heat conduction terms are added to the conservation equations of mass, momentum, and energy, respectively. The improved equations are [19, 20]:

$$\frac{\partial \rho_i}{\partial t} + \nabla \cdot (\rho_i \boldsymbol{u}) = -\nabla \cdot (\rho_i \boldsymbol{u}_{\mathrm{di}}), \tag{2}$$

$$\frac{\partial \rho \boldsymbol{u}}{\partial t} + \nabla \cdot (\rho \boldsymbol{u}\boldsymbol{u}) = \nabla \cdot \tau - \nabla p, \tag{3}$$

$$\begin{aligned} &\frac{\partial \rho \left(e + \dfrac{\boldsymbol{u}^2}{2}\right)}{\partial t} + \nabla \cdot \left(\rho \left(e + \frac{\boldsymbol{u}^2}{2}\right)\boldsymbol{u}\right) \\ &= \nabla \cdot (\tau \cdot \boldsymbol{u}) - \nabla \cdot (p\boldsymbol{u}) - \nabla \cdot \boldsymbol{q} - q^{\mathrm{rad}} + (\alpha_{\mathrm{IB}} + \alpha_{\mathrm{PI}}) I. \end{aligned} \tag{4}$$

where ρ_i, ρ, $\boldsymbol{u}$, p, e and q^{rad} are the mass density of species i, total mass density, expansion velocity, local pressure, specific internal energy, and power loss [19], respectively, $\boldsymbol{u}_{\mathrm{di}}$, τ and $\boldsymbol{q}$ are the diffusion velocity of species i [21], viscous stress tensor, and heat conduction flux [20], and α_{IB} and α_{PI} are the inverse bremsstrahlung absorption coefficient and photoionization coefficient [22].

2.3. Decontamination of bacteria

The plasma generated by laser ablation of the target material continues to expand outward until its edges come into contact with the surface of the plate to be decontaminated. Subsequently, all the energy of the plasma acts on the bacteria, inactivating them through the high-energy particles carried inside. Figure 1 shows a schematic diagram of bacterial decontamination by laser-induced plasma, where d is the distance from the center of the plate to the target surface, and θ is the angle between the plate and the horizontal plane.

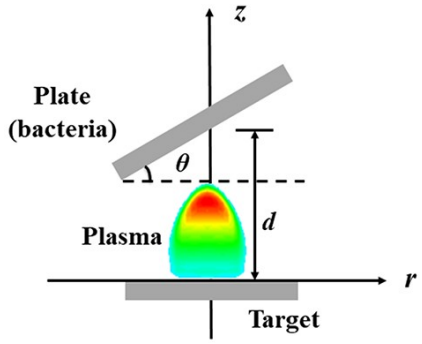

Figure 1. Schematic diagram of bacterial decontamination on the plate surface by laser-induced plasma.

3. Results and discussion

3.1. Effect of laser parameters on decontamination

This section focuses on the influence of laser spot size and wavelength on the laser-induced plasma decontamination effect. After laser ablation of the target material, the generated plasma rapidly expands outward. Figure 2 shows the simulation results of plasma energy density profiles under the same laser pulse energy but with different spot sizes, at a delay time of 0.5 μs. Here, plasma energy refers to the sum of internal energy and kinetic energy, and its density reaches a maximum at the top edge of the plasma. Due to the presence of background gas, a compressed shock wave is formed at the front of the plasma. In this region, the vapor plasma collides with the background gas to exchange energy, creating a significant gradient in energy density that decreases rapidly. At the minimum laser spot, the maximum laser irradiance is observed. After 0.5 μs of evolution, the axial and radial dimensions of the plasma also show a trend of maximization. This result is consistent with the experimental conclusion of Conesa *et al* that plasma size increases with increasing irradiance [23]. In addition, as the laser irradiance decreases, the plasma profile is compressed from spherical to ellipsoidal along the axial direction, indicating that laser irradiance has a significant impact on the axial size of the plasma. When the same total laser energy acts on the target material, the increase in spot size leads to a decrease in laser energy density, resulting in a decrease in the energy density of the formed plasma. For example, if the spot radius

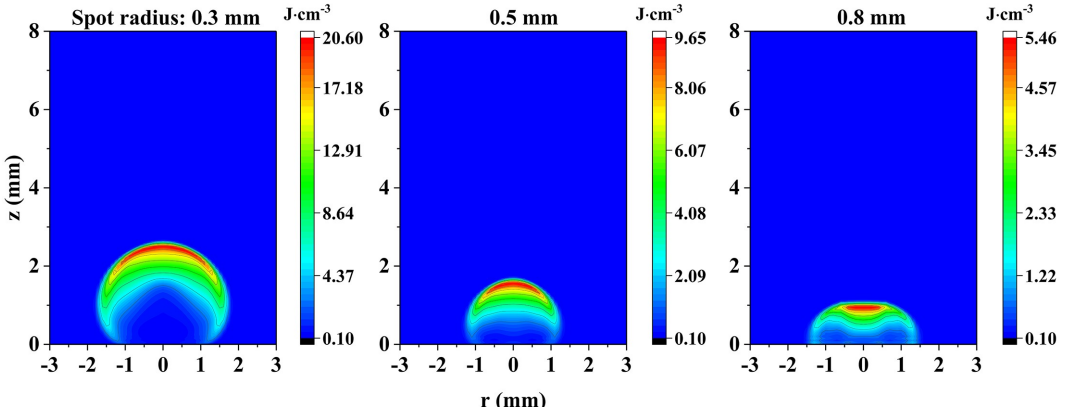

Figure 2. Energy density profiles of plasma at 0.5 μs under the same laser pulse energy and different spot sizes.

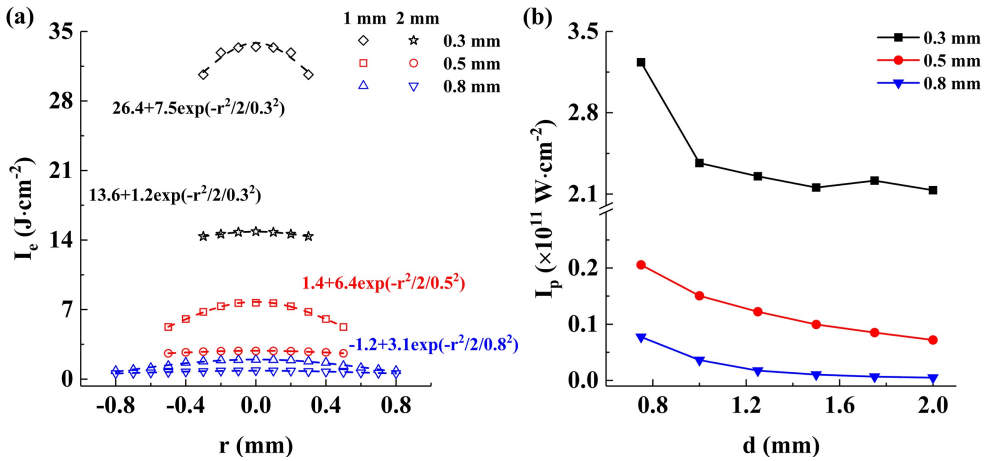

Figure 3. Radial distribution of bombardment energy density (a) and relationship between bombardment power density and plate-target spacing (b) under different spot sizes ($\theta = 0°$).

increases from 0.3 mm to 0.8 mm, the maximum plasma energy density decreases from 20.58 J/cm^3 to 5.46 J/cm^3. Overall, changes in laser irradiance can significantly affect the size and energy density of the plasma.

The plasma generated by laser ablation rapidly expands outward and decontaminates the plate coated with bacteria. Figure 3(a) shows the radial distribution of plasma energy density I_e under different spot sizes r and plate-target spacing d. The scattered points represent the theoretical simulation results, and the curves are exponential fitting results with correlation coefficients R^2 greater than 0.90. The fitting equation used is $y = a+b\exp(-x^2/2r^2)$, where x is the radial position. This equation characterizes the energy distribution of plasma bombardment on bacteria, which exhibits a Gaussian-like distribution along the radial direction. When the plate is parallel to the target material, the bombardment energy is maximum at the center of the spot and minimum at the boundary. Especially at a large spot size, the coefficient b is small, indicating a reduction in energy difference between the center and the boundary, and a more uniform distribution of bombardment energy within the spot range. However, as the size of the spot increases, the energy density of the plasma decreases, and the energy acting on the bacteria also decreases accordingly. It can be seen that in order to improve the decontamination efficiency of plasma on bacteria, it is necessary to increase the power density of the laser. On the contrary, reducing the laser power density can improve the uniformity of decontamination. When the plate-target spacing increases from 1 mm to 2 mm, the expansion time of the plasma increases, resulting in more energy loss and a decrease in the energy acting on the bacteria. Figure 3(b) shows the quantitative relationship between bombardment power density I_p and plate-target spacing d under different spot sizes. As spot size and spacing increase, the bombardment power gradually decreases, consistent with the results in figure 3(a). This indicates that by reducing the size of the laser spot and the plate-target spacing, the bombardment characteristics of the plasma can be effectively controlled, thereby achieving better bacterial decontamination effects.

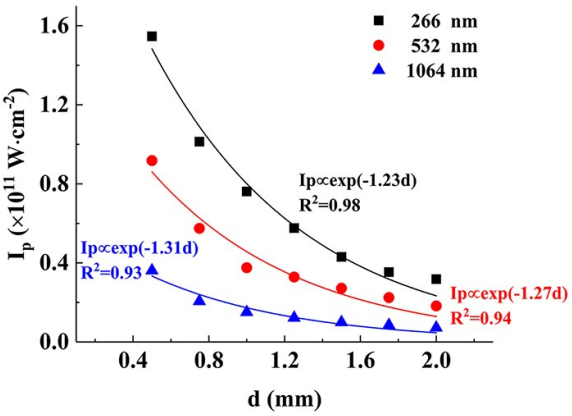

Figure 4. Relationship between power density of plasma bombardment and plate-target spacing under different laser wavelengths ($\theta = 0°$).

Figure 4 illustrates the relationship curve between bombardment power density and plate-target spacing under different laser wavelength conditions when the spot radius is 0.5 mm. The scattered points represent the theoretical simulation results, while the solid lines depict the fitted curves, with R^2 greater than 0.93. The power density of plasma bombardment on bacteria decreases exponentially with increasing plate-target spacing. Under the same laser power density and target material conditions, the shorter the laser wavelength, the higher the electron number density and electron temperature of the generated plasma, resulting in a greater bombardment power of plasma on bacteria and a more effective decontamination effect. This theoretical simulation conclusion aligns with the reported results. Bogaerts *et al* theoretically confirmed that at 1 atm of helium, the parameters of the plasma generated by short-wavelength laser (266 nm) ablation of the copper target were greater than those of long-wavelength laser (1064 nm) [24]. The comparative experiment of short-wavelength (355 nm) and long-wavelength (1064 nm) laser-induced aluminum plasma conducted by Ma *et al* in 1 atm argon also confirmed this conclusion [25]. The fitting exponential formulas are also annotated in the figure, and the constant term in parentheses reflects the rate at which bombardment power decreases with

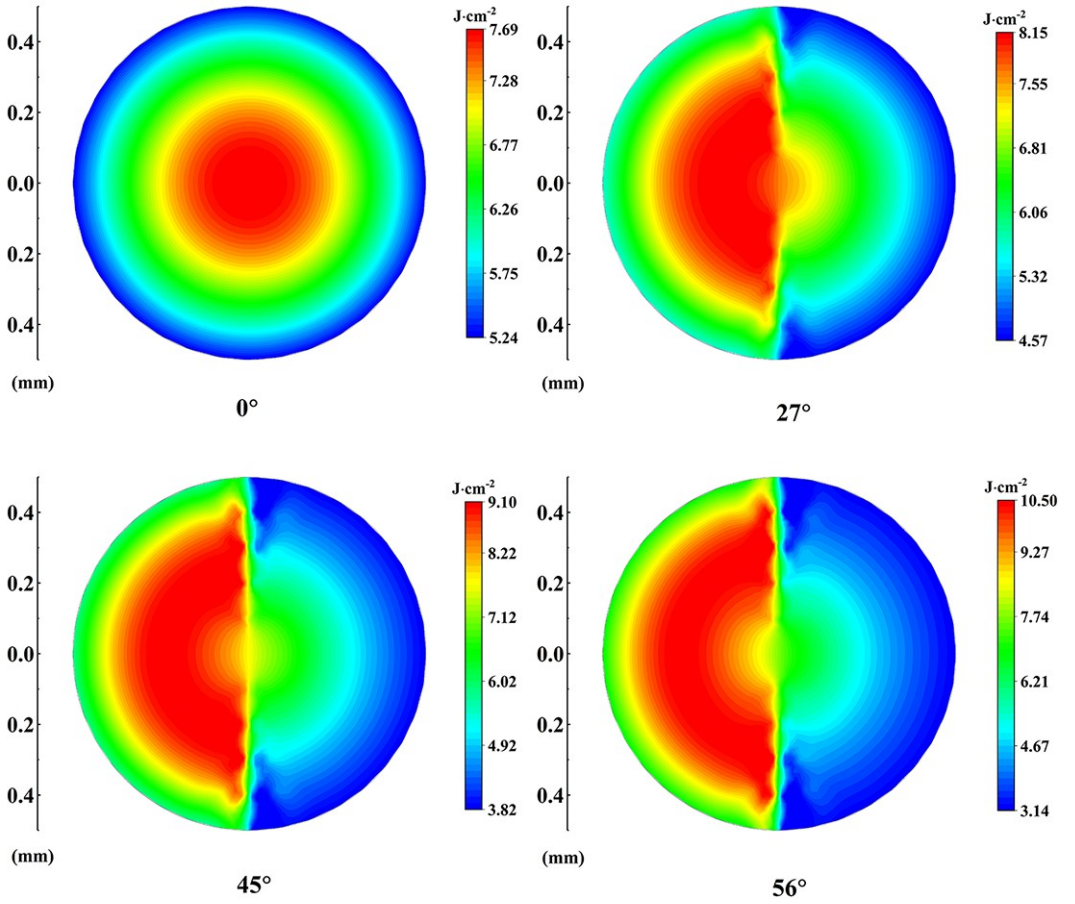

Figure 5. Energy density profiles of plasma bombardment on bacteria at different tilt angles (d = 1 mm, r = 0.5 mm).

spacing. In other words, the smaller the constant, the slower the decrease in bombardment power. The shorter the laser wavelength, the slower the decrease in bombardment power with increasing spacing. This indicates that the laser wavelength has a significant impact on the plasma decontamination effect, and a decrease in wavelength is beneficial for bacterial decontamination.

3.2. Effect of plate's tilt angle on decontamination

In addition to laser parameters, we also investigate the impact of the plate's tilt angle on the efficiency of bacterial decontamination. Figure 5 shows the energy density profiles of plasma bombardment on bacteria at different tilt angles when d = 1 mm and r = 0.5 mm. At the angle of 0°, the energy of the plasma acting on the bacteria is centrally symmetric, with the bombardment energy density gradually decreasing from the center to the edge. This distribution is determined by the particles sputtered in the plasma and follows a Gaussian-like distribution. Consequently, as the plasma continues to deposit on the plate, the formed energy distribution also exhibits a similar Gaussian-like pattern. When there is a certain angle between the plate and the target material, the energy density distribution of the plasma acting on the bacteria shows obvious non-uniformity. The left half is closer to the target surface than the right half, resulting in greater bombardment energy. As the tilt angle

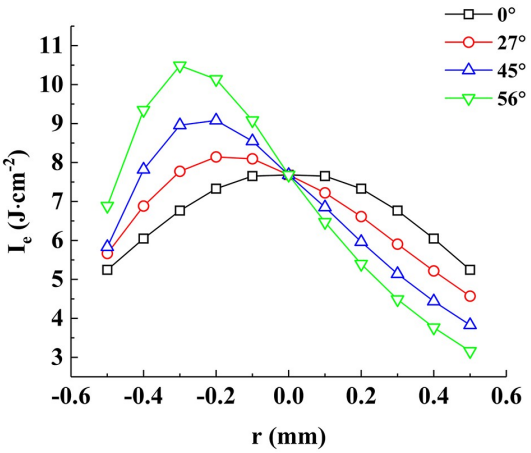

Figure 6. Radial distribution of bombardment energy density acting on bacteria at different tilt angles (d = 1 mm, r = 0.5 mm).

increases, the energy density of plasma bombardment increases in the left half, while it decreases in the right half. The energy density distribution in the left and right parts becomes more uneven. Figure 6 displays the radial distribution of energy density corresponding to figure 5 when d = 1 mm and r = 0.5 mm. It can be observed that the bombardment energy density of the plasma at the center (r = 0 mm) remains the same at different tilt angles. However, as the tilt angle increases, the peak energy density gradually shifts from the center of the spot to the left, and the difference in bombardment energy density between the left and right parts

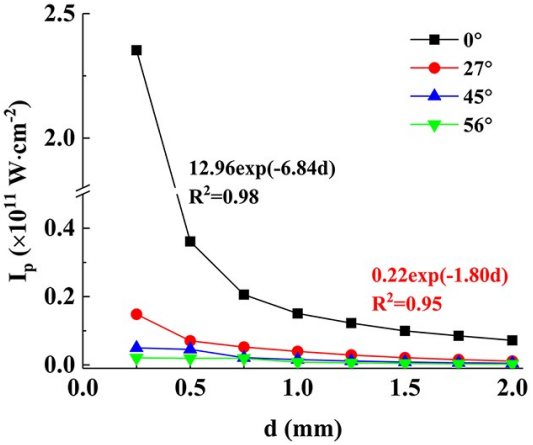

Figure 7. Relationship between power density of plasma bombardment acting on bacteria and the plate-target spacing at different tilt angles (r = 0.5 mm).

of the plasma also becomes more significant. For example, when the angle increases from 0° to 56°, the maximum energy density difference in the radial direction increases from 2.44 J/cm^2 to 7.33 J/cm^2. These observations indicate that the tilt angle of the plate has a significant impact on the energy density distribution of plasma, consequently affecting the effectiveness of bacterial decontamination. By adjusting the tilt angle of the plate, precise control of plasma bombardment energy density can be achieved.

Figure 7 shows the relationship between bombardment power density and plate-target spacing at different tilt angles. Overall, the power density tends to decrease with the increase in plate-target spacing and tilt angle. When the plate is parallel to the target surface (θ = 0°), the bombardment power reaches its maximum value. As the plate tilts continuously, the bombardment power gradually decreases, even if the bombardment energy of the plasma in the local area is greater. At larger spacing, the bombardment power is almost the same at all angles except for θ = 0°. The tilt angle of the plate has almost no effect on the bombardment power density of the plasma acting on bacteria. When the tilt angle is less than 45° and the spacing is less than 0.5 mm, the bombardment power initially decreases rapidly with the increase in spacing, and then tends to flatten. When the tilt angle is greater than 45°, the decreasing trend of bombardment power with the increase in spacing is relatively slow. This suggests that when the plate is tilted beyond a certain angle, the bombardment power density is almost independent of the spatial position of the plate. Similarly, the fitted exponential expressions are annotated in the figure, and the exponential function can well describe the evolution trend between bombardment power and plate-target spacing.

4. Conclusion

In this study, we utilize an advanced fluid dynamics model to simulate and access the effectiveness of plasma generated by pulse laser with different parameters in decontaminating bacteria on the plate placed at different spatial positions. Emphasizing the destructive impact of high-speed moving particles on bacteria, we evaluate the decontamination efficiency of plasma on bacteria through power density of plasma bombardment. The study explores the evolution of power density concerning laser spot size, wavelength, plate's tilt angle, and plate-target spacing. The findings reveal that reducing the laser spot size and wavelength can generate plasma with higher species density and temperature, thereby increasing the bombardment power of plasma acting on bacteria and enhancing its decontamination effect. Taking the example of a plate parallel to the target surface with a spacing of 1 mm, the bombardment power density increases approximately threefold when the laser spot size decreases from 0.8 mm to 0.5 mm, and about fourfold when the wavelength decreases from 1064 nm to 266 nm. The tilt angle of the plate and the distance from the target also affect the power density of plasma bombardment on bacteria. Smaller tilt angles and closer proximity to the target result in greater bombardment power of the plasma on bacteria, leading to improved decontamination effects. When the tilt angle is below 45° and the spacing is less than 0.5 mm, the power density of plasma bombardment significantly increases, rising by 1–46 times compared to 45°. This simulation study provides valuable insights for the further advancement of decontamination technology. Optimal laser parameters and device layout can be selected to optimize and control the decontamination process more effectively, facilitating precise bacterial decontamination.

Acknowledgments

This work was supported by National Key R&D Program of China (No. 2017YFA0304203), National Energy R&D Center of Petroleum Refining Technology (RIPP, SINOPEC), Changjiang Scholars and Innovative Research Team in University of Ministry of Education of China (No. IRT_17R70), National Natural Science Foundation of China (Nos. 12374377, 61975103 and 627010407), 111 Project (No. D18001), Fund for Shanxi '1331KSC'.

References

[1] Sun Y *et al* 2016 *Int. Biodeter. Biodegr.* **112** 119
[2] Wang X *et al* 2020 *J. Water Reuse Desal.* **10** 82
[3] Cantwell R E and Hofmann R 2008 *Water Res.* **42** 2729
[4] Jia Q *et al* 2013 *Food Sci.* **34** 61
[5] Wrigley D M and Llorca N G 1992 *J. Food Protect.* **55** 678
[6] Cai W *et al* 2019 *Guangdong Agr. Sci.* **46** 99
[7] Park D K, Bitton G and Melker R 2006 *J. Environ. Health* **69** 17
[8] Wang Z *et al* 2016 *Front. Phys.* **11** 114213
[9] Guo L *et al* 2021 *Front. Phys.* **16** 22500
[10] Shukla S *et al* 2006 *Proc. SPIE* **6084** 608417
[11] Grishkanich A *et al* 2016 *Proc. SPIE* **9709** 97090U
[12] Terlep S *et al* 2022 *Lasers Med. Sci.* **37** 381
[13] Jang H *et al* 2022 *Ceram. Int.* **48** 1446
[14] Kawasaki H *et al* 2015 *4th International Congress on Advanced Applied Informatics* DOI: 10.1109/IIAI-

AAI.2015.204
[15] Kawasaki H *et al* 2016 *Trans. Mater. Res. Soc. Jpn.* **41** 205
[16] Mi Z *et al* 2023 *Anal. Methods* **15** 297
[17] Liang J *et al* 2023 *J. Photoch. Photobio. B* **244** 112719
[18] Bhattacharya D, Singh R K and Holloway P H 1991 *J. Appl. Phys.* **70** 5433
[19] Chen Z Y and Bogaerts A 2005 *J. Appl. Phys.* **97** 063305
[20] Wang J X *et al* 2023 *Opt. Express* **31** 16423
[21] Oran E S and Boris J P 1987 *Numerical Simulation of Reactive Flow* (New York: Elsevier)
[22] Wang J *et al* 2022 *Plasma Sci. Technol.* **24** 035005
[23] Conesa S, Palanco S and Laserna J J 2004 *Spectrochim. Acta B* **59** 1395
[24] Bogaerts A and Chen Z 2005 *Spectrochim. Acta B* **60** 1280
[25] Ma Q *et al* 2012 *J. Appl. Phys.* **111** 053301